RSC Advances

PAPER

View Article Online
View Journal | View Issue

Cite this: *RSC Adv.*, 2018, **8**, 37277

Optimized cesium and potassium ion-exchanged zeolites A and X granules for biogas upgrading†

Kritika Narang,[a] Kristina Fodor,[a] Andreas Kaiser[b] and Farid Akhtar *[a]

Received 26th September 2018
Accepted 26th October 2018

DOI: 10.1039/c8ra08004f

rsc.li/rsc-advances

Partially ion-exchanged zeolites A and X binderless granules were evaluated for CO_2 separation from CH_4. The CO_2 adsorption capacity and CO_2-over-CH_4 selectivity of binderless zeolites A and X granules were optimized by partial exchange of cations with K^+ and Cs^+, while retaining the mechanical strength of 1.3 MPa and 2 MPa, respectively. Single gas CO_2 and CH_4 adsorption isotherms were recorded on zeolites A and X granules and used to estimate the co-adsorption of CO_2–CH_4 using ideal adsorbed solution theory (IAST). The IAST co-adsorption analysis showed that the partially ion-exchanged binderless zeolites A and X granules had a high CO_2-over-CH_4 selectivity of 1775 and 525 respectively, at 100 kPa and 298 K. Optimally ion-exchanged zeolite X granules retained 97% of CO_2 uptake capacity, 3.8 mmol g^{-1}, after 5 breakthrough adsorption–desorption cycles while for zeolite A ion-exchanged granules the reduction in CO_2 uptake capacity was found to be 18%; CO_2 uptake capacity of 3.4 mmol g^{-1}. The mass transfer analysis of breakthrough experimental data showed that the ion-exchanged zeolite X had offered a higher mass transfer coefficient, (κ) through the adsorption column compared to zeolite A; 0.41 and 0.13 m s^{-1} for $NaK_{4.5}Cs_{0.3}X$ and $CaK_{2.5}Cs_{0.2}A$, respectively.

Introduction

The combustion of biomass produces approximately the same amount of CO_2 with respect to its decomposition cycle, which leads to biomass carbon neutrality. In this respect, biomass conversion to biogas is a viable choice of a renewable fuel.[1] Biogas is produced from a large diversity of biomass feedstocks, such as sewage, industrial waste, agricultural waste, dairy manure, landfill waste, food processing by products, *etc.*, *via* anaerobic digestion.[2] Methane is the primary component of raw biogas (45–75%) in addition to carbon dioxide (typically 25–55%) and other components like hydrogen sulfide, ammonia, water and trace gas compounds like oxygen and hydrocarbons.[3] In order to use biogas as vehicle fuel or its induction to existing natural gas grids, upgrading of biogas to biomethane with a CH_4 mole fraction over 96% is required to meet the standards laid out by respective industries.[4] Several technologies have been developed to upgrade raw biogas *via* adsorption[5] absorption,[6] permeation[7] and cryogenic technologies[8] resulting in biogas with a content of CH_4 > 90%.[9] Moreover, adsorption-based technologies offer advantages like low upgrading costs and ease of scalability with biogas production unit over other technologies.

Various microporous adsorbents have been explored during the last two decades in the field of biogas upgrading such as activated carbon, zeolites and metal–organic frameworks (MOFs).[10] Zeolites A and X have many advantageous properties like flexibility in tailoring the pore opening, high CO_2 uptake capacity, chemical and thermal stability, hence these materials have been investigated for biogas and natural gas upgrading.[11–13] Analogues of zeolite A with 8-ring pore openings have pore apertures with the diameters similar to the kinetic diameters of CO_2 (0.33 nm), N_2 (0.364 nm) and CH_4 (0.38 nm).[14] The aperture size for zeolite A depends on the extra framework cation present in the structure, thus it varies between 0.3–0.5 nm.[15] Due to these characteristics, researchers have tailored the pore size using partial ion exchange process on zeolite A for CO_2 separation from gas streams.[16] Liu *et al.*, ion exchanged Na^+ cations with K^+ and reported ideal CO_2-over-N_2 selectivity of 172 with 17 atomic percentage (at%) K^+ content in zeolite A.[15] Bacsik *et al.*, investigated NaKA zeolites for CO_2-over-CH_4 separation, and suggested that $|Na_{12-x}K_x|$-LTA, with x ranging between 1.8 $\leq x \leq$ 3.2 (x being the number of ions in pseudocell) offers high CO_2-over-CH_4 selectivity.[17] Cheung *et al.*, reported a high CO_2-over-CH_4 selectivity, of around 1500 for $|Na_{10.2}KCs_{0.8}|$-LTA, which was achieved by partial ion exchanging Na^+ to K^+, and then replacing some of the K^+ with Cs^+.[18] Zeolite NaX has been studied extensively for CO_2 separation from flue-gas streams due to its superior CO_2 adsorption capacity and selectivity over N_2.[19–21] Harlick and Tezel showed that NaX and NaY had the highest CO_2 adsorption capacities and proposed these zeolites as best candidates for CO_2 separation,[22] while Walton *et al.*,

[a]*Division of Materials Science, Luleå University of Technology, Luleå 97187, Sweden. E-mail: farid.akhtar@ltu.se*

[b]*Department of Energy Conversion, Technical University of Denmark, Roskilde 4000, Denmark*

† Electronic supplementary information (ESI) available. See DOI: 10.1039/c8ra08004f

showed that in all cases X zeolites possess more CO_2 molecules per supercage than the Y by examining their Li, K, Na, Rb, and Cs ion exchanged derivatives.[23] Next to this, Cavenati *et al.*, conducted a study of high pressure adsorption of CO_2, CH_4 and N_2 on zeolite NaX, and concluded that the adsorbent was highly selective to CO_2 thus rendering it suitable for purification purposes.[20]

The microporous zeolites are used in structured forms in adsorption-based separation technologies using pressure and/or temperature cycling. The mechanically stable structured microporous materials are required to minimize the pressure drop, promote high gas flow and rapid mass transfer kinetics throughout the adsorption column in a swing adsorption process.[24] The earlier reports on the partially ion-exchanged are focused on powdered zeolite. The processing of these partially ion-exchange powders to structured forms using clay binders (typically 25–45%)[25] can influence the adsorption properties significantly.[26] Moreover, the addition of clay binders to zeolites to achieve desired mechanical stability reduces the durability of the structured product.[27] The reports on structuring of partially ion-exchange zeolites are sparse despite the fact that structuring is an important aspect of practical separation of CO_2 from methane for biogas upgrading using adsorption-based technologies.[28] In this regard, current work reports a robust method to process partially ion-exchange binderless structured granules of zeolite CaA and NaX with reasonably high mechanical stability and adsorption performance for biogas upgrading. The binderless granules of zeolite CaA and NaX were subjected to partial ion-exchange with K^+ and Cs^+ cations to optimize the adsorptive properties for CO_2 separation from CH_4 in a pressure swing adsorption process. The evaluation of adsorption properties such as CO_2 uptake capacity, CO_2-over-CH_4 selectivity and cyclic performance of mechanically strong partially ion-exchanged zeolites A and X granules are reported. Cyclic breakthrough measurements and calculated mass transfer coefficients of zeolite NaX and CaA granules as well as their optimal ion exchanged derivatives are reported in this study to evaluate the performance.

Experimental

Materials and methods

Commercially available zeolite NaX and CaA powder and binderless granules were purchased from Luoyang Jianlong Chemical Industrial Co. Ltd., Yanshi, Henan, China, with zeolite crystal size 2–4.5 μm. Potassium chloride (optical grade 99%) and cesium chloride (optical grade ≥99.5%) were purchased from Sigma Aldrich Chemie GmBH, Germany. The partial ion exchange is a simple and a robust method. The K^+ and Cs^+ ion exchange process for the granules was performed in two stages. First, the CaA and NaX zeolite granules were partially ion-exchanged by K^+ cations and then the partially K^+ exchanged zeolite granules (CaKA and NaKX) were collected and further ion exchanged with Cs^+ cations. The detailed experimental description of the ion exchange process on the powders of zeolite NaX and CaA and their CO_2/CH_4 selectivities are provided in the ESI (Tables 1S and 2S,† respectively). The optimum combination of CO_2 uptake capacity and CO_2/CH_4 selectivity obtained from the partially K^+ and Cs^+ ion exchanged powders of zeolite CaA and NaX was used as a guideline to prepare partially K^+ and Cs^+ ion exchanged granules of CaA and NaX to obtain optimum combination of CO_2 uptake capacity and CO_2-over-CH_4 selectivity as shown in Table 1.

Characterization

The elemental composition of the partial ion exchanged NaX and CaA powders as well as of granules were determined by energy dispersive spectroscopy (EDS) using JEOL JCM-6000Plus scanning electron microscope (SEM). The zeolites granules were crushed into powder and were spread onto a double-sided copper tape and examined at an accelerating voltage of 15 kV.

Table 1 Ion exchange process description for NaX and CaA powder and granules

Starting zeolite	Amount of zeolite (g)	Amount of KCl (g)	Amount of CsCl (g)	Amount of water (ml)	Stirring time (min)	Final zeolite composition[a]
NaX powder						
NaX	5	1	—	500	30	$NaK_{3.7}X$
$NaK_{3.7}X$	1.2	—	0.02	120	30	$NaK_{3.27}Cs_{0.19}X$
NaX granule						
NaX	10	8	—	1000	60	$NaK_{3.9}X$
$NaK_{3.9}X$	5	—	0.20	500	60	$NaK_{4.5}Cs_{0.3}X$
CaA powder						
CaA	1	0.8	—	100	30	$CaK_{3.4}A$
$CaK_{3.4}A$	1.8	—	0.06	180	30	$CaK_{2.5}Cs_{0.45}A$
CaA granule						
CaA	5.1	4	—	1000	60	$CaK_{2.6}A$
$CaK_{2.6}A$	5.9	—	0.20	500	60	$CaK_{2.5}Cs_{0.2}A$

[a] The final composition of the zeolite after ion-exchange was determined by EDS analysis.

The same procedure was followed for the zeolite powders. Scanning electron microscope (SEM) micrographs were obtained on JEOL JSM-IT300 microscope. The X-ray powder diffraction pattern (PXRD) of NaX, CaA zeolites including its ion-exchange derivatives were analyzed using PANalytical's X-ray diffractometer (Empyrean, Nederland) over the 2θ range from 5 to 60°.

The CO_2, CH_4 equilibrium adsorption isotherms were collected on a Gemini VII 2390 Surface Area Analyzer (Micromeritics, Norcross, USA). Apart from the adsorption isotherms, the surface area of the samples was measured by N_2 adsorption at liquid nitrogen temperature (77 K) using Brunauer–Emmett–Teller analysis technique. Prior to the measurements, the specimens were degassed using VacPrep 061 for 24 h at 573 K under a dynamic vacuum. All the adsorption measurements were done at 298 K within a pressure range of 1 to 90 kPa. The CO_2-over-CH_4 selectivities of all zeolites were calculated using Henry's Law constants (K_H) and ideal adsorbed solution theory. The co-adsorption of CO_2–CH_4 was estimated using ideal adsorbed solution theory (IAST). Single gas adsorption data and Langmuir model were utilized to obtain the parameters needed to estimate the binary selectivity coefficients using IAST model for a mixed gas containing 50–50 mol% of CO_2–CH_4 at various total pressures. The equilibrium cyclic performance of the ion-exchanged zeolites was recorded on a Gemini VII 2390 Surface Area Analyzer (Micromeritics, Norcross, USA).

The mechanical strength of the granules was determined by performing a compression test between the steel plates in a 1 kN load cell on Zwick Z050 universal test machine. A pre-load of 5 N was used. The test was carried out on five identical granules of each type to obtain a statistically significant data distribution. Mercury intrusion porosimetry of the zeolites granules was performed on a Micromeritics AutoPore III-9400 (Norcross, GA, USA) over a wide range of pressures (0.03–420 MPa). The pore size distributions were obtained from the Washburn equation using 0.485 N m^{-1} surface tension and 130° contact angle of mercury. To investigate the biogas upgrading, cyclic breakthrough measurements on NaX, CaA granules as well as their potassium and cesium ion exchange analogues were obtained using a Pressure Swing Adsorption PSA-300LC (L&C Science and Technology, Florida, USA) system. Prior to the measurement, the zeolite granules were regenerated at 200 °C in helium gas passing through the column at a flow rate of 20 ml min^{-1} for 12 h. Moreover, the dew point of −15 °C was used as a benchmark to ensure the drying of the zeolite column. A binary mixture of CO_2/CH_4 (45 mol%/55 mol%) gas was passed in the fixed bed of length 100 mm and 15 mm in diameter to study the adsorption performance of zeolites and its optimum ion exchange derivatives at 2 bar and 293 K up to 5 cycles. The flow rate was set to 19 ml min^{-1} and 15 ml min^{-1} for CO_2 and CH_4 gases respectively. The amount of the adsorbent in the PSA column were 4.96 g, 5.30 g, 4.28 g, 4.70 g for NaX, CaA, optimal ion exchanged NaX, optimal ion exchanged CaA zeolites, respectively. For the cyclic measurements, the zeolite column was regenerated by evacuation. A pressure of 0.01 bar was chosen to be reached in the columns for regeneration in the cyclic measurements.

Results and discussion

The zeolite granules, 1.6 mm in diameter, in Fig. 1 consist of primary zeolite particles with a size distribution of 2.5 to 4.0 microns for CaA granules and 2.5 to 4.5 microns for NaX granules. The partial ion-exchanged derivatives of zeolites CaA and NaX granules with K^+ and Cs^+ were prepared following the adsorptive properties and energy dispersive spectroscopy analysis of elemental composition of partial ion exchange of CaA and NaX powders with varying fraction of K^+ and Cs^+ cations (ESI, Table 3S†). The compositions of the optimal ion exchange zeolite A and X granules determined from energy dispersive spectroscopy (EDS) analysis were $CaK_{2.6}A$, $CaK_{2.5}Cs_{0.2}A$, $NaK_{3.9}X$ and $NaK_{4.5}Cs_{0.3}X$, respectively. The microstructure and X-ray diffraction data in Fig. 1 and ESI (Fig. 1S and 2S†) confirms that the optimal ion exchanged zeolite A and X crystals preserve the morphology and crystallinity after the ion exchange process.

In (Fig. 2a), the uptake capacities of CO_2 of zeolite CaA and ion-exchanged $CaK_{2.5}Cs_{0.2}A$ granules are 4.5 mmol g^{-1} and 4.3 mmol g^{-1}, respectively. In (Fig. 2b), the uptake capacity of CO_2 for zeolite NaX and $NaK_{4.5}Cs_{0.3}X$ granules are 5.6 mmol g^{-1} and 5.1 mmol g^{-1}, respectively. The CO_2 uptake capacity of binderless granules of CaA and NaX is comparable to the structured zeolite A and X monoliths prepared without addition of binders.[25,29,30] Moreover, it has been established that the binderless structured adsorbents offer advantages of high CO_2 adsorption capacity and durability over traditional adsorbents structured using inorganic clay binders up to 45% to achieve the mechanical strength.[27,31] After partial ion-exchange, the binderless zeolite granules show small decrease in the uptake capacities, which is attributable to the presence of extra framework cations. The charge density decreases in order of Na > K > Cs, resulting in a decrease of electrostatic interaction between the extra frameworks cations and the permanent quadruple moment of CO_2 and hence the reduction in CO_2 capacities is observed for the optimal ion-exchanged granules. Similar decrease in the CO_2 uptake capacity was shown by the partially ion exchange CaA and NaX powders (ESI, Fig. 3S†). This result agrees with studies of Walton *et al.*, who showed that the CO_2 capacity increased with the small alkali cations in X and Y zeolites.[23] Similar results have been reported in the literature on alkali exchanged faujasite zeolites.[32] The CO_2 uptake capacities for the ion exchanged zeolite granules are higher than the previously reported ion exchanged zeolites,[18] 3D-printed NaX and CaA zeolite monoliths[29] while maintaining the high CO_2/CH_4 selectivity of the granules.

In (Fig. 2a), the CH_4 adsorption capacities of zeolite CaA and optimal ion-exchanged $CaK_{2.5}Cs_{0.2}A$ granules are 0.74 mmol g^{-1} and 0.69 mmol g^{-1}, respectively and in (Fig. 2b), the uptake capacity of CH_4 for zeolite NaX and $NaK_{4.5}Cs_{0.3}X$ granules are 0.67 mmol g^{-1} and 0.46 mmol g^{-1}, respectively. The reduction in CH_4 uptake is connected to the hindrance to the percolation of CH_4 due to enhanced diffusion barrier in ion-exchanged cages.[33] The partial ion exchange of the CaA and NaX powders shows the similar reduction in CH_4 adsorption capacities (ESI, Fig. 4S†). Moreover, linear isotherms were obtained in case of

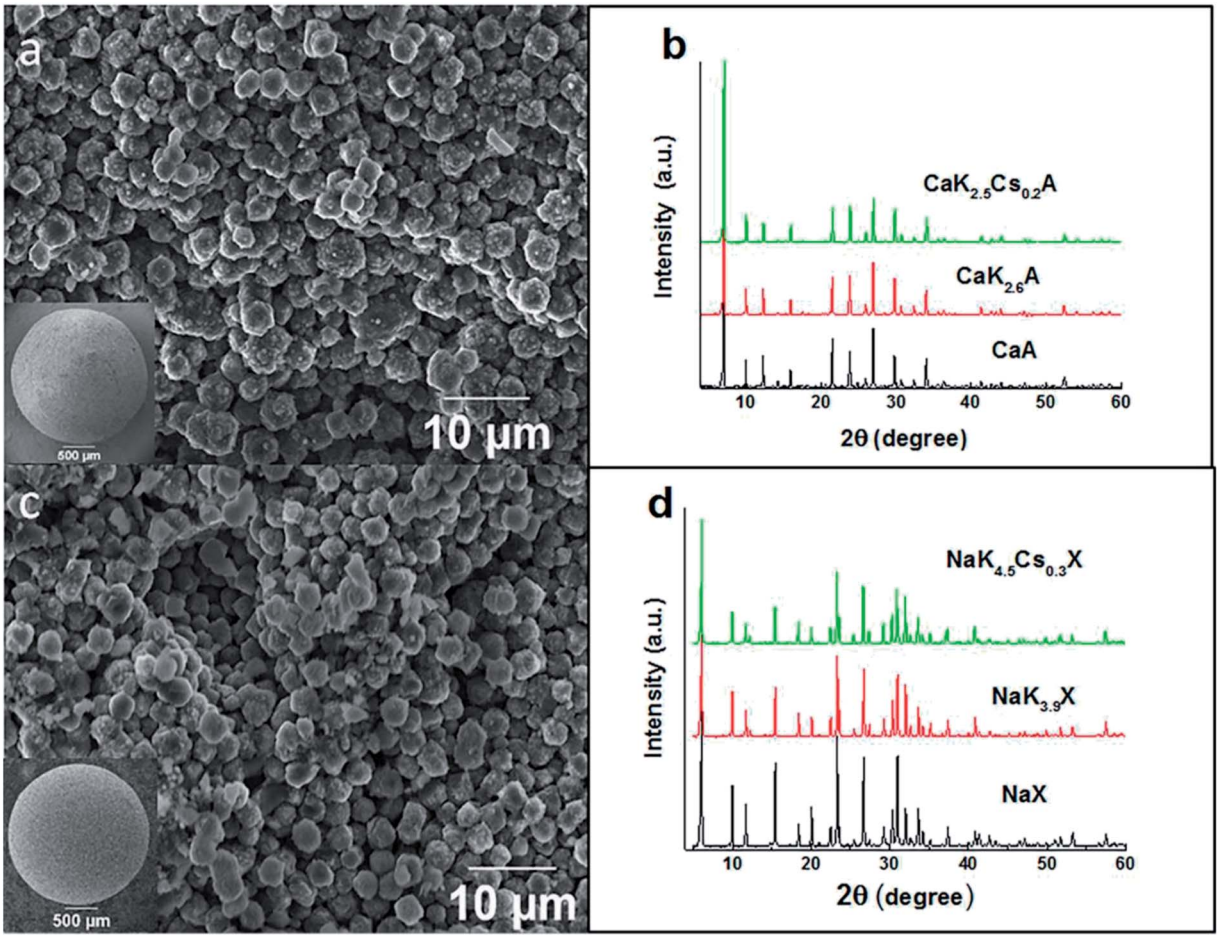

Fig. 1 (a) SEM of CaA granules with inset of CaA granule (b) XRD of CaA granules (as-received CaA granules, $CaK_{2.6}A$ and $CaK_{2.5}Cs_{0.2}A$) (c) SEM of NaX granules with inset of NaX granule (d) XRD of NaX granules (as-received NaX granules, $NaK_{3.9}X$ and $NaK_{4.5}Cs_{0.3}X$).

CH_4 adsorption due to the absence of a quadruple moment in CH_4 giving rise to weak interaction primarily *via* dispersion–repulsion forces exist between CH_4 molecules and the adsorbent.[34] CO_2 cyclic adsorption isotherms for the optimal ion exchange derivatives of CaA and NaX granules are reported in (Fig. 2c and d) respectively. The cyclic stability was investigated over up to 4 cycles. For the first cycle, the zeolite granules were regenerated at 300 °C under vacuum and for the further cycles, the zeolites were regenerated under vacuum at room temperature.

In (Fig. 2c and d), the reduction in the CO_2 adsorption capacity is observed after cycle 1. The reason for this reduction is attributed to chemisorption of CO_2.[35,36] No further reduction is observed in the following cycles. For the $CaK_{2.5}Cs_{0.2}A$ granules, 15% of the reduction in the CO_2 uptake is noticed from 1st cycle to 4th cycle, while the reduction of 7.9% is observed in the case of $NaK_{4.5}Cs_{0.3}X$ granules. However, after the first cycle, the $CaK_{2.5}Cs_{0.2}A$ and $NaK_{4.5}Cs_{0.3}X$ granules keep the CO_2 adsorption capacity.

The textural properties and the CO_2-over-CH_4 selectivity of zeolites granules and the optimal ion exchange derivatives are shown in Table 2. The specific surface areas of granulated $CaK_{2.5}Cs_{0.2}A$ and $NaK_{4.5}Cs_{0.3}X$ are 351 $m^2\ g^{-1}$ and 474 $m^2\ g^{-1}$, respectively. The decrease in the surface area is observed with the increase of cation size (Na < K < Cs), as reported earlier.[37] The external surface area and the micropore volume of the $NaK_{4.5}Cs_{0.3}X$ granules were 33 $m^2\ g^{-1}$ and 0.25 $cm^3\ g^{-1}$ and for $CaK_{2.5}Cs_{0.2}A$ granules were 64.2 $m^2\ g^{-1}$ and 0.16 $cm^3\ g^{-1}$ respectively. There is no significant decrease in micropore volume and external surface area for the zeolites with its corresponding optimal ion exchange derivatives. These results suggest that the ion-exchange process of zeolite granules did not result in surface contamination of the zeolite particles and the granules. The reduction in the total surface area is mainly determined by the reduction in micropore area due to size difference of the cations. Similar observations have been reported for ion exchanged zeolite powders.[38,39] The calculated CO_2-over-CH_4 selectivities in Table 2, using Langmuir adsorption model and ideal adsorbed solution theory (IAST), show higher values for optimal ion-exchanged zeolites CaA and NaX with K^+ and Cs^+ cations (ESI, Table 4S† for Langmuir parameter and the Henry's constant for the powders and granules). The CO_2-over-CH_4 selectivity increases with partial exchange of K^+ cations. It is also noticed, that the CO_2-over-CH_4 selectivity increased with the addition of Cs^+ in the structure. The role of the Cs^+ in the structure is determined to be two-fold. First, due

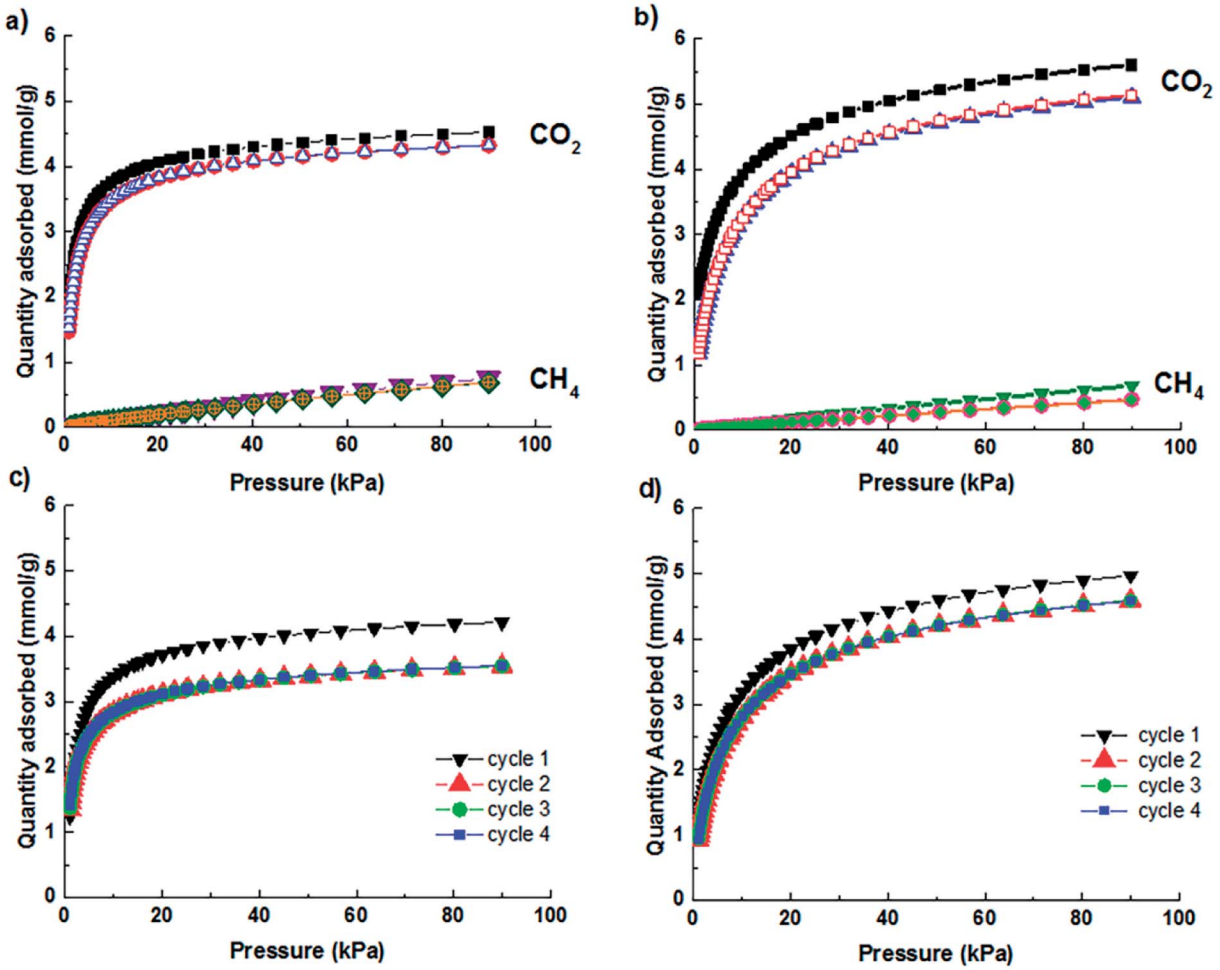

Fig. 2 (a) CO_2 adsorption isotherms of CaA granules: as-received (■ black square), $CaK_{2.6}A$ (● red circle) and $CaK_{2.5}Cs_{0.2}A$ (△ blue hollow triangle), and CH_4 adsorption isotherms of CaA granules: as-received (▼ purple inverted triangle), $CaK_{2.6}A$ (◆ dark green diamond) and $CaK_{2.5}Cs_{0.2}A$ (⊕ orange circle with plus sign inside). (b) CO_2 adsorption isotherms of NaX granules: as-received (■ black square), $NaK_{3.9}X$ (▲ blue triangle) and $NaK_{4.5}Cs_{0.3}X$ (□ red hollow square), and CH_4 adsorption isotherms of NaX granules: as-received (▼ olive inverted triangle), $NaK_{3.9}X$ (● pink circle) and $NaK_{4.5}Cs_{0.3}X$ (◆ green diamond). (c) cyclic adsorption of CO_2 on $CaK_{2.5}Cs_{0.2}A$ granules. (d) Cyclic adsorption of CO_2 on optimized $NaK_{4.5}Cs_{0.3}X$ granules: cycle 1 (▼ black inverted triangle), cycle 2 (▲ red triangle), cycle 3 (● green circle), cycle 4 (■ blue square).

to its size it is expected to reduce the pore opening of the super cage to achieve molecular sieving effect, however the significant size difference of Cs^+ compared to Na^+ ion will generate a stronger interaction for the bigger cation, because the molecular shielding from the surrounding oxygen atoms is less, thus the interaction with CH_4 will not be limited, as it is the case with the Na^+.[40]

Furthermore, it is deduced that two factors will affect the selectivity of the potassium and cesium ion-exchanged zeolite granules: (a) steric selectivity, due to the reduced pore opening and pore volume and (b) the difference in the interactions of CO_2 and CH_4 gases with the individual cations. Even though zeolite NaX contains cations at all sites, position I and I′ are within the sodalite cages and these are usually not reachable for

Table 2 Textural properties of CaA and NaX zeolites and their optimal ion exchange derivatives, including the IAST selectivities

Granules	BET surface area ($m^2\ g^{-1}$)	Micropore area ($m^2\ g^{-1}$)	External surface area ($m^2\ g^{-1}$)	Micropore volume ($cm^3\ g^{-1}$)	IAST selectivity (CO_2/CH_4)
CaA	436	370	66.6	0.21	542
$CaK_{2.6}A$	354	304	50.1	0.17	906
$CaK_{2.5}Cs_{0.2}A$	351	287	64.2	0.16	1773
NaX	496	461	35	0.26	329
$NaK_{3.9}X$	458	425.4	32.8	0.24	384
$NaK_{4.5}Cs_{0.3}X$	474	441.4	33	0.25	525

Table 3 Macroporosity and mechanical strength of the CaA and NaX and their ion exchanged derivatives

Granules	Macroporosity (%)	Compressive strength (MPa)
CaA	24.7	3 ± 0.7
$CaK_{2.6}A$	25	3.6 ± 1.1
$CaK_{2.5}Cs_{0.2}A$	29.2	1.3 ± 0.4
NaX	21	4.4 ± 2.0
$NaK_{3.9}X$	23	3.4 ± 0.9
$NaK_{4.5}Cs_{0.3}X$	19.5	2 ± 0.4

most adsorbate molecule (ESI, Fig. 5S†).[23] The non-accessibility of certain sites due to the size difference of the cations leads to a significant decrease in CH_4 uptake of the cesium and potassium ion exchanged zeolites, generating only a slight reduction in the CO_2 uptake. This difference in the amount of reduction in the CH_4 and CO_2 uptake capacities give rise to high CO_2-over-CH_4 selectivity. The interaction between the cations and the CO_2 is higher as compared CH_4 due to the stronger polarizability and quadrupole moment of CO_2.[41]

The use of zeolites in industrial applications requires a strong macroscopic structure with good mechanical stability and hierarchical porosity which can provide a low pressure drop and rapid mass transfer kinetics.[42] High mechanical strength is crucial for the adsorbents as they undergo large and rapid pressure and thermal variations.[27,43] Table 3 shows that the mechanical strength of the optimal ion-exchanged granules is comparable to pure CaA and NaX granules. Nevertheless, a drop in the mechanical strength has been noticed for the optimal cesium ion exchanged granules. Optimal cesium exchanged granules underwent two times the ion exchange process which may result in erosion and dissolution of contact points/bridges between the zeolite crystals in the granules and reduce the mechanical strength.[31] The mechanical strength of ion-exchanged binderless CaA and NaX granules (Table 3) is higher than the mechanical strength reported for conventional structured CaA and NaX zeolite monoliths.[25] The retention of mechanical strength after the ion-exchange process is related to the binderless nature of the zeolite granules. It has been reported that the addition of clay binders to the zeolites results in significant reduction in the mechanical durability of the structured body on exposure to acidic and basic aqueous media.[27]

Fig. 3 shows the differential pore size distribution of the CaA, NaX and its optimal ion exchange derivative, measured by mercury porosimetry. The macroporosity of the zeolites is listed in Table 3. The CaA and the NaX zeolite granules show a homogeneous pore size distribution with a maximum centered at 0.4 μm. The peak corresponds to interparticle voids between the zeolites particles in the binderless granules. Such large pores are required for efficient mass transfer of gas molecules to the adsorption sites in the zeolite crystals.

Fig. 4 shows the cyclic breakthrough experiments on adsorption column of binderless CaA and NaX granules and their optimum ion exchanged derivatives to evaluate and compare the performance. In breakthrough curve, C/C_0 implies relative concentration of CO_2, where C and C_0 represent the concentration at the outlet and the inlet of the fixed bed respectively. The first part of the breakthrough curve in which the relative concentration (C/C_0) is zero implies that all the CO_2 gas molecules are being adsorbed. The second part of the curves with a steep increase in relative concentration implies that the adsorbent is saturated, and an increasing concentration of CO_2 gas molecules is slipping (through the column). The zone between zero to one is described as mass transfer zone (MTZ). The fixed bed is completely saturated when C/C_0 is equal to one.

After the first cycle, the reduction in the breakthrough point for further cycles is due to the chemisorbed CO_2 molecules, as observed in cyclic experiment in (Fig. 2c and d) also, that could not be released through regeneration by evacuation. Both of the optimal ion exchange zeolite granules show stability in the adsorption capacity after three cycles. The amount of CO_2 adsorbed by the zeolites until the breakthrough point for pure NaX and CaA zeolites were determined to be 4.6 mmol and

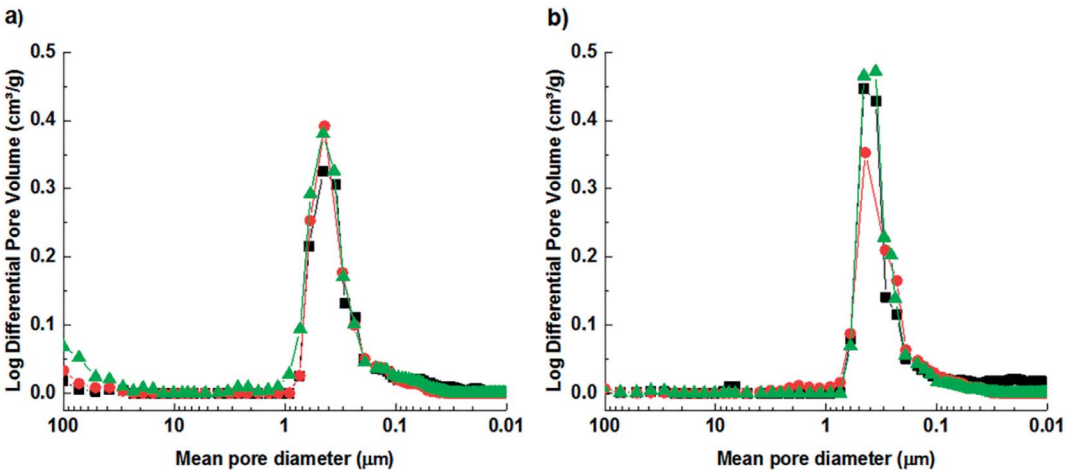

Fig. 3 (a) Pore size distribution of CaA granules of as-received granules (square), $CaK_{2.6}A$ (circle) and $CaK_{2.5}Cs_{0.2}A$ (triangle). (b) Pore size distribution of NaX granules of as-received granules (square), $NaK_{3.9}X$ (circle) and $NaK_{4.5}Cs_{0.3}X$ (triangle).

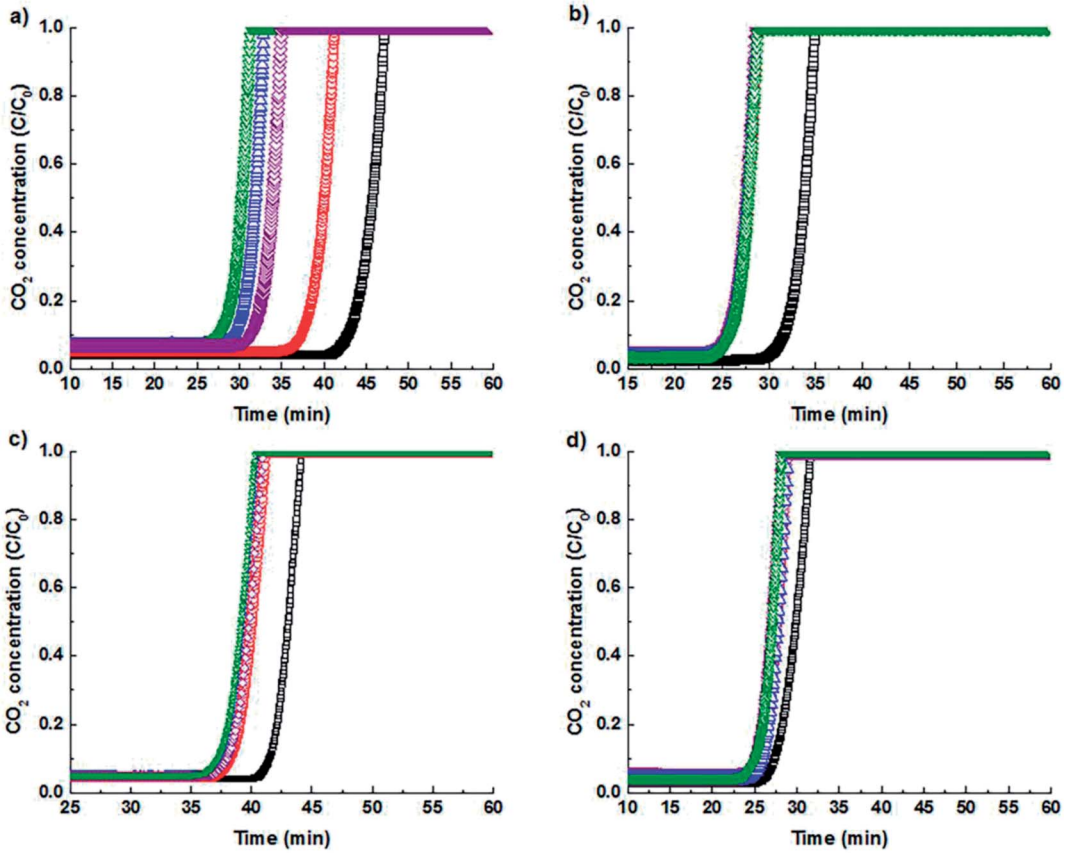

Fig. 4 CO_2 cyclic breakthrough measurements on (a) CaA granules, (b) $CaK_{2.5}Cs_{0.2}A$ granules, (c) NaX granules and (d) $NaK_{4.5}Cs_{0.3}X$ granules (□ black cycle 1, ○ red cycle 2, ◇ purple cycle 3, △ blue cycle 4, ▽ green cycle 5).

3.3 mmol of CO_2 per g of the zeolite, respectively, for the final cycle. $NaK_{4.5}Cs_{0.3}X$ shows the adsorption capacity of 3.8 mmol g^{-1} in the final cycle and is higher than the $CaK_{2.5}Cs_{0.2}A$ zeolite, which adsorbs 3.4 mmol of CO_2 per g of zeolite.

The CO_2 uptake rate was 2.8 mg of CO_2 per g per s for $NaK_{4.5}Cs_{0.3}X$ and 2.5 mg of CO_2 per g per s for $CaK_{2.5}Cs_{0.2}A$ granules. The amount of CO_2 adsorbed in breakthrough experiment is less than the amount adsorbed in the equilibrium gas adsorption experiment shown in Fig. 2. The sharp front in the breakthrough curve as shown in Fig. 4 implies that the zeolite granules have low mass transfer resistance and the fluid flow distribution is even within the granules. The mass transfer coefficient which corresponds to the speed of the molecules to diffuse and amount adsorb within the adsorbent can be derived from eqn (1) which was adapted from Klinkenberg[44] and was fitted to the experimental breakthrough.

$$C/C_0 = 1/2 \times erfc\left(7\sqrt{\xi}\Big/8 - 9\sqrt{\tau}/8\right) \quad (1)$$

where ξ is the dimensionless length given by eqn (2) and τ is the dimensionless time given by eqn (3).

$$\xi = \kappa Kz((1-\varepsilon)/\upsilon\varepsilon) \quad (2)$$

$$\tau = \kappa\left(t - \frac{z}{\upsilon}\right) \quad (3)$$

$$\upsilon = \frac{Q_V\varepsilon}{S} \quad (4)$$

In above equations, κ is mass transfer coefficient, K is Henry constant of the adsorbate, ε is the total void fraction, z is the bed length, t is the time in minutes, υ is interstitial velocity which is given by eqn (4), where Q_V is the volumetric flow rate of the gas and S is the cross-sectional surface area of the bed.

The simulated mass transfer coefficient κ is 1.01 and 0.6 m s^{-1} for pure NaX and CaA granules, respectively. High mass transfer indicates rapid diffusion of CO_2 molecules into the adsorbent. The mass transfer is fast in NaX due to relatively large pore size (0.74 nm) in the zeolite framework. The mass transfer coefficient was reduced to 0.41 and 0.13 m s^{-1} for $NaK_{4.5}Cs_{0.3}X$ and $CaK_{2.5}Cs_{0.2}A$ granules respectively. Due to the presence of extra framework cations in the zeolite, the diffusion of CO_2 molecules is slower in the adsorbents and hence resulted in the relatively low mass transfer coefficient. The mass transfer coefficients for pure and ion-exchanged derivates are comparable to laminated NaA zeolites prepared by freeze casting.[28]

Conclusions

The optimal ion exchange of CaA and NaX zeolites and their adsorption properties were studied. The optimal concentration

was determined according to the performance of the ion exchange zeolites by evaluating the CO_2-over-CH_4 selectivity using IAST theory. The CaKCsA with the 2.5 (at%) K^+ and 0.2 (at%) Cs^+ content and NaKCsX with the 4.5 (at%) K^+ and 0.3 (at%) Cs^+ content gives the CO_2 uptake value of 4.3 mmol g^{-1} and 5.1 mmol g^{-1} respectively with high CO_2-over-CH_4 selectivity as compared to pure CaA and NaX. The optimal ion exchanged CaA and NaX zeolites shows high mechanical strength of 1.3 MPa and 2 MPa respectively. The breakthrough curves suggest low mass transfer resistance for both NaX and CaA granules including its optimal ion exchanged derivatives. NaX ion exchange granules have shown better performance as compared to CaA ion exchange zeolite, by having a CO_2 uptake rate of 2.8 mg of CO_2 per g per s while achieving the stability after few cycles with a mass transfer coefficient of 0.41 m s^{-1}.

Conflicts of interest

There are no conflicts to declare.

Acknowledgements

The authors acknowledge the Innovation Fund Denmark (grant no. 5157-00008A), Formas (grant no. 2016–01099), Kempestiftelserna (grant no. JCK 1437) for their financial support. The authors acknowledge Hanzhu Zhang for the help in the experimental work.

References

1 A. Whiting and A. Azapagic, *Energy*, 2014, **70**, 181–193.
2 Ş. Y. Balaman and H. Selim, *Appl. Energy*, 2014, **130**, 289–304.
3 Q. Zhao, E. Leonhardt, C. MacConnell, C. Frear and S. Chen, *CSANR Research Report*, 2010, **9**, 1–24.
4 M. Scholz, T. Melin and M. Wessling, *Renewable Sustainable Energy Rev.*, 2013, **17**, 199–212.
5 M. P. S. Santos, C. A. Grande and A. E. Rodrigues, *Ind. Eng. Chem. Res.*, 2011, **50**, 974–985.
6 O. I. Maile, E. Muzenda and H. Tesfagiorgis, *Procedia Manufacturing*, 2017, **7**, 639–646.
7 X. Y. Chen, H. Vinh-Thang, A. A. Ramirez, D. Rodrigue and S. Kaliaguine, *RSC Adv.*, 2015, **5**, 24399–24448.
8 A. M. I. Yousef, Y. A. Eldrainy, W. M. El-Maghlany and A. Attia, *Alexandria Eng. J.*, 2016, **55**, 1143–1150.
9 L. Deng and M. Hägg, *Int. J. Greenhouse Gas Control*, 2010, **4**, 638–646.
10 T. A. Makal, J. Li, W. Lu and H. Zhou, *Chem. Soc. Rev.*, 2012, **41**, 7761–7779.
11 T. Montanari, E. Finocchio, E. Salvatore, G. Garuti, A. Giordano, C. Pistarino and G. Busca, *Energy*, 2011, **36**, 314–319.
12 S. J. Chen, Z. C. Tao, Y. Fu, M. Zhu, W. L. Li and X. D. Li, *Appl. Energy*, 2017, **205**, 1435–1446.
13 Y. Gao, J. Zhou, H. Sheng, X. Liu, X. Yong, S. Wang, Z. Yan and T. Zheng, *Xiandai Huagong*, 2014, **34**, 50–54.
14 R. T. Yang, *Adsorbents: Fundamentals and Applications*, WileyInterscience, New York, 2003.
15 Q. Liu, A. Mace, Z. Bacsik, J. Sun, A. Laaksonen and N. Hedin, *Chem. Commun.*, 2010, **46**, 4502–4504.
16 B. Yang, Y. Liu and M. Li, *Chin. Chem. Lett.*, 2016, **27**, 933–937.
17 Z. Bacsik, O. Cheung, P. Vasiliev and N. Hedin, *Appl. Energy*, 2016, **162**, 613–621.
18 O. Cheung, D. Wardecki, Z. Bacsik, P. Vasiliev, L. B. McCusker and N. Hedin, *Phys. Chem. Chem. Phys.*, 2016, **18**, 16080–16083.
19 D. Ko, R. Siriwardane and L. Biegler, *Ind. Eng. Chem. Res.*, 2003, **42**, 339–348.
20 S. Cavenati, C. A. Grande and A. E. Rodrigues, *J. Chem. Eng. Data*, 2004, **49**(4), 1095–1101.
21 A. Eskandari, M. Jahangiri and M. Anbia, *Int. J. Eng., Trans. A*, 2016, **29**, 1–7.
22 P. J. E. Harlick and F. H. Tezel, *Microporous Mesoporous Mater.*, 2004, **76**, 71–79.
23 K. S. Walton, M. B. Abney and M. D. LeVan, *Microporous Mesoporous Mater.*, 2006, **91**, 78–84.
24 F. Rezaei and P. Webley, *Chem. Eng. Sci.*, 2009, **64**, 5182–5191.
25 F. Akhtar and L. Bergström, *J. Am. Ceram. Soc.*, 2011, **94**, 92–98.
26 R. V. Jasra, B. Tyagi, Y. M. Badheka, V. N. Choudary and T. S. G. Bhat, *Ind. Eng. Chem. Res.*, 2003, **42**, 3263–3272.
27 F. Akhtar, L. Andersson, S. Ogunwumi, N. Hedin and L. Bergström, *J. Eur. Ceram. Soc.*, 2014, **34**, 1643–1666.
28 A. Ojuva, M. Järveläinen, M. Bauer, L. Keskinen, M. Valkonen, F. Akhtar, E. Levänen and L. Bergström, *J. Eur. Ceram. Soc.*, 2015, **35**, 2607–2618.
29 H. Thakkar, S. Eastman, A. Hajari, A. A. Rownaghi, J. C. Knox and F. Rezaei, *ACS Appl. Mater. Interfaces*, 2016, **8**, 27753–27761.
30 F. Akhtar, Q. Liu, N. Hedin and L. Bergström, *Energy Environ. Sci.*, 2012, **5**, 7664–7673.
31 N. Keshavarzi, F. Akhtar and L. Bergström, *J. Mater. Res.*, 2013, **28**, 2253–2259.
32 S. Salehi and M. Anbia, *J. Inorg. Organomet. Polym. Mater.*, 2017, **27**, 1281–1291.
33 T. Remy, E. Gobechiya, D. Danaci, S. A. Peter, P. Xiao, L. Van Tendeloo, S. Couck, J. Shang, C. E. A. Kirschhock, R. K. Singh, J. A. Martens, G. V. Baron, P. A. Webley and J. F. M. Denayer, *RSC Adv.*, 2014, **4**, 62511–62524.
34 Q. Jiang, J. Rentschler, G. Sethia, S. Weinman, R. Perrone and K. Liu, *Chem. Eng. J.*, 2013, **230**, 380–388.
35 B. P. Spigarelli and S. K. Kawatra, *J. CO2 Util.*, 2013, **1**, 69–87.
36 L. Bertsch and H. W. Habgood, *J. Phys. Chem.*, 1963, **67**, 1621–1628.
37 G. P. Dangi, K. Munusamy, R. S. Somani and H. C. Bajaj, *Indian J. Chem., Sect. A: Inorg., Bio-inorg., Phys., Theor. Anal. Chem.*, 2012, **51**, 1238–1251.
38 N. Sue-aok, T. Srithanratana, K. Rangsriwatananon and S. Hengrasmee, *Appl. Surf. Sci.*, 2010, **256**, 3997–4002.
39 S. Yang, J. Kim and W. Ahn, *Microporous Mesoporous Mater.*, 2010, **135**, 90–94.
40 G. Sethia, R. S. Somani and H. C. Bajaj, *Ind. Eng. Chem. Res.*, 2014, **53**, 6807–6814.

41 F. Akhtar, N. Keshavarzi, D. Shakarova, O. Cheung, N. Hedin and L. Bergström, *RSC Adv.*, 2014, **4**, 55877–55883.
42 P. Vasiliev, F. Akhtar, J. Grins, J. Mouzon, C. Andersson, J. Hedlund and L. Bergström, *ACS Appl. Mater. Interfaces*, 2010, **2**, 732–737.
43 F. Akhtar, S. Ogunwumi and L. Bergström, *Sci. Rep.*, 2017, **7**, 10988.
44 A. Klinkenberg, *Ind. Eng. Chem.*, 1954, **46**, 2285–2289.